Bulletin of the New Zealand Society for Earthquake Engineering, Vol. 55, No. 2, June 2022

INCREMENTAL DYNAMIC ANALYSIS OF RIGID BLOCKS SUBJECTED TO GROUND AND FLOOR MOTIONS AND SHAKE TABLE PROTOCOL INPUTS

Danilo D'Angela[1], Gennaro Magliulo[2] and Edoardo Cosenza[3]

(Submitted *March 2021*; Reviewed *May 2021*; Accepted *October 2021*)

ABSTRACT

This paper reports the results of an extensive campaign of incremental dynamic analyses (IDA) of rigid rocking blocks under various loading histories, including real ground/floor motions and shake table testing protocol loading histories. Several block geometries are investigated considering various size and slenderness combinations representative of building contents, monumental elements, art objects, components of critical facilities, and other unanchored elements. The spectral response of the block to different loading histories is firstly assessed by highlighting the characteristics of the different seismic input sets. Dimensionless acceleration- and velocity-based parameters are considered as intensity measures, and the block rotation normalized considering the critical angle (i.e., dimensionless rocking amplitude) is assumed as an engineering demand parameter. The IDA curves are evaluated, and the dynamic response of the blocks is characterized in terms of: (a) type of loading history, (b) intensity measure, and (c) block geometry.

New information and technical insights are presented regarding the assessment of seismic response of structural and nonstructural rocking systems. The dynamic response of the blocks subjected to the investigated protocols is found to be not always compatible with the capacities related to real ground/floor motions, often producing non-conservative estimations. The discrepancy identified between the block responses associated with the protocol inputs and real motions is found to be significantly affected by both block geometry and intensity measure.

INTRODUCTION

Structural and nonstructural elements of various types of engineering systems are often not connected to their supports by means of mechanical devices, or their fastening systems have a negligible influence on their dynamic response when subjected to moderate to high intensity shaking (e.g., [1,2]). These elements are often critically sensitive to the seismic demand in terms of accelerations, so they are typically classified as acceleration-sensitive [3]. Unanchored (or freestanding) and ineffectively fastened systems include but are not limited to geological structures [4,5], monumental or historical structures and museum elements [6–10], parts of (infra)structural systems [11–13], laboratory and hospital equipment [1,14–16], nuclear and power plant equipment [16,17], and generic building contents [18–20]. The seismic risk related to these types of elements can be critically high, as such elements are typically associated with high vulnerability and exposure, as well as they can be located in moderate to high hazard sites (e.g., [2,21]). This is more critical for nonstructural elements that are hosted by special buildings and critical facilities that have to guarantee post-event operation and community resilience [22,23]. Figure 1 depicts the post-event seismic damage of critical unanchored elements (2016 Amatrice earthquake, Italy): (a) overturning of beverage stocks, and (b) rigid dislocation of the pinnacle of the *San Benedetto Basilica.* In both cases, a rigid-body motion was observed. This behavior can cause major damage and human losses. For example, rocking-dominated damage of masonry buildings and churches (quite widespread in earthquake-prone countries) can be potentially life-threatening [10,24], besides causing critical cultural losses.

Figure 1: Post-earthquake damage (after the 24/08/16 Amatrice earthquake, Italy) of critical unanchored elements: (a) overturning of beverage stocks; and (b) rigid dislocation of the pinnacle of the San Benedetto Basilica.

The seismic response of unanchored (or freestanding) and ineffectively anchored elements can be often modeled considering the rigid motion approach. When the freestanding elements are relatively slender, and the friction coefficient is sufficiently high to prevent sliding response (e.g., [25,26]), the dynamics of rigid blocks can be assumed to be dominated by the rocking motion [19,27]. The dynamics of rocking blocks has been studied since early times, and the seminal study of Housner [28] laid the foundations of the so-called *classical theory*, by providing the equations of the rigid block motion. Several early pioneering studies implemented and extended the rigid block motion analysis to evaluate the dynamic response of various elements under different loading histories (e.g., [29–33]).

[1] *Research fellow, University of Naples Federico II, Naples*
[2] *Corresponding Author, Professor, University of Naples Federico II, Naples* gmagliul@unina.it
[3] *Professor, University of Naples Federico II, Naples*

More recently, the efficiency and reliability of the Housner modeling approach were corroborated by means of shake table testing and statistical-based evaluation (e.g., [5,14,19,34]). Several studies addressed the issue by extending the analytical investigation to more peculiar applications and providing insights into the assessment of the seismic response of rocking systems [6,35–38]. Some researchers [5,19,27,34,39] focused on the record-to-record variability of the rigid block response, which is among the most critical aspects associated with the rocking behavior (e.g., [34]).

Despite the copious literature addressing the rocking motion of structural and nonstructural systems, there are still critical aspects that have not been fully investigated. For instance, very few studies investigated the rocking response of freestanding elements subjected to floor motions, which can be representative of the typical case of building equipment, contents, and secondary systems supported by buildings (e.g., roof structures that house tanks or electric equipment). Recently, Fragiadakis and Diamantopoulos [18] investigated the seismic response of building contents hosted in a four-story RC building by means of numerical analyses, providing a framework for performance-based assessment. They highlighted the complexity of the issue and stressed the gap in the literature. The response of building contents under floor motions should be further investigated. As a matter of fact, the buildings act as a filter and condition both acceleration amplification and frequency content associated with the seismic demands on the nonstructural elements housed in buildings (i.e., through floor motions). The influence of this filtering action on the seismic behavior of rocking elements has never been directly addressed in the literature, especially considering representative sets of ground and floor motions. Moreover, the response of rigid blocks under shake table protocol inputs should also be investigated since these loading histories are typically used to seismically qualify (and certify) acceleration-sensitive components, including freestanding systems. The use of such protocol inputs was addressed in the literature by the preliminary study of Burningham et al. [40]. Considering only a block geometry, the most referenced protocols (AC156 [41] and FEMA 461 [42]) were found to potentially overestimate the overturning acceleration in terms of fragility curves, considering floor motions as a reference and peak (floor) acceleration as an intensity measure (IM). Accordingly, this might result in potential non-conservative estimations if the fragility curves are assumed as component capacities (e.g., [43,44]). Similar observations were also expressed in recent studies (e.g., [43,45,46]).

This study reports the results of an extended campaign of incremental dynamic analyses (IDAs) of rigid blocks subjected to a variety of loading histories, i.e., real ground motions (ATC-63 [47]), real floor motions (CESMD [48]), and inputs developed according to reference shake table protocols (AC156 [41], FEMA 461 [42], and Wittich and Hutchinson [45]). A wide range of block geometries is analyzed, and dimensionless floor and ground acceleration- and velocity-based IMs are considered [27].

NUMERICAL ANALYSES

IDAs of rigid blocks were carried out by solving the Housner equations of motion [28] using the Runge-Kutta ordinary differential equation (ODE) solver in MATLAB [49]. The maximum acceleration of the seismic input at the base of the block (a_{max}) was considered as an incremental IM, whereas the absolute value of the peak block rotation to critical angle ratio ($|\theta_{max}/\alpha|$) was assumed as an engineering demand parameter (EDP). Several block geometries were analyzed under various loading histories.

.

Rigid Block Modeling

The geometrical parameters of rigid blocks are shown in Figure 2, where R is the semi-diagonal dimension (Equation (1)), often named block size, θ is the block rotation, h/b is the slenderness, α is the critical angle (Equation (2)), and p is the frequency parameter (Equation (3), where g is the acceleration due to gravity). The pure rocking response was modeled in this study, assuming a friction coefficient sufficiently high to prevent sliding. This assumption is often made in the literature for blocks that are relatively slender, like the ones investigated in this study [6,19,25,27,50]. Therefore, the block motion can be fully described by its oscillation about the base corners (O and O' in Figure 2). Equation (4) reports the equation of motion related to a rigid block excited by an acceleration loading history $\ddot{u}_g(t)$. Equation (5) describes the coefficient of restitution e, which is defined as the ratio between the post- and pre-impact angular velocity. According to Housner [28], e can be defined assuming that the post- to pre-impact angular velocity reduction follows the angular momentum balance [51]. A unitary coefficient of restitution e was assumed to produce conservative and generalizable estimations [14,19].

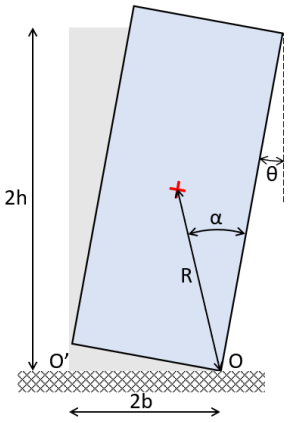

Figure 2: Geometry of the rigid block.

$$R = \sqrt{b^2 + h^2} \tag{1}$$

$$\alpha = \tan^{-1}\left(\frac{b}{h}\right) \tag{2}$$

$$p = \sqrt{\frac{3g}{4R}}; \tag{3}$$

$$\ddot{\theta}(t) = -p^2\left\{\sin\left[\alpha\,\mathrm{sgn}(\theta(t)) - \theta(t)\right] + \frac{\ddot{u}_g(t)}{g}\cos\left[\alpha\,\mathrm{sgn}(\theta(t)) - \theta(t)\right]\right\} \tag{4}$$

$$e = 1 - \frac{3}{2}\sin^2\alpha \tag{5}$$

Block Geometries

Two sets of block geometries were analyzed: set 1 is related to small-to-medium size blocks [1] (e.g., building contents) and set 2 is related to medium-to-large block sizes [29] (e.g., monumental elements and secondary systems). The block geometries are depicted in Figure 3 and reported in Table 1.

Table 1: Investigated block geometries.

		Set 1					Set 2				
Block ID		**#1A**	**#1B**	**#1C**	**#1D**	**#1E**	**#2A**	**#2B**	**#2C**	**#2D**	**#2E**
R	**[m]**	0.36	0.72	0.72	0.72	1.43	1.52	3.05	3.05	3.05	4.57
h/b	**[-]**	3.92	1.96	3.92	7.83	3.92	5	2.5	5	7.5	5
α	[-]	0.250	0.472	0.250	0.127	0.250	0.197	0.381	0.197	0.133	0.197

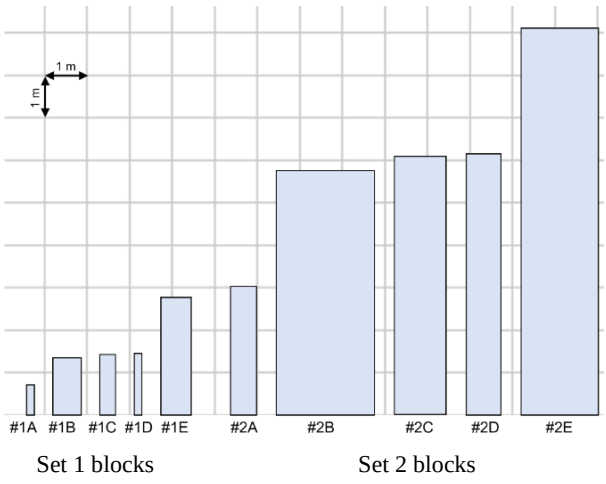

Figure 3: Geometries of the investigated blocks.

Loading Histories

Three types of records were considered as analysis loading histories: real ground motions (GM set or GMs), real floor motions (FM set or FMs), and shake table protocol inputs (STPI set or STPIs). GM set was derived from the ATC-63 database [47] and included records having magnitude larger than 6.5, peak ground acceleration (PGA) larger than 0.20 g, and peak ground velocity (PGV) larger than 15 cm/s. In particular, 44 far-field records (GM FF sub-set) and 28 near-field records (GM NF sub-set) were considered. The related time histories were also used in other studies (e.g., [19,52]).

FM set includes accelerograms recorded within instrumented US RC buildings, which were derived from the Center for Engineering Strong Motion Data (CESMD) database [48]. The selected records are related to ground motions having PGA larger than 0.05 g. In particular, the set includes floor records related to 12 near-field records (FM NF sub-set, i.e., FM #1-12) and 12 far-field records (FM FF sub-set, i.e., FM #13-24) registered in different buildings. For each earthquake, the most amplified building floor response provided by the database was selected (larger a_{max}). For the sake of representativeness of the considered FM set and sub-sets, each sub-set includes the same number of motions recorded within low-rise, medium-rise, and high-rise buildings (corresponding to FM #1-4,13-16, FM #5-8,17-20, and FM #9-12,21-24). Figure 4 depicts the time history accelerations ($a(t)$) related to FM inputs, scaled in order to have a_{max} equal to 1.0 g. The signals were scaled considering a_{max} since this IM is typically used in similar contexts (e.g. [19,43]) and was also used for the implementation of the incremental analyses. The same value of a_{max} was chosen to favor correct comparisons among the different inputs. The specific value of 1.0 g was used since this ease the graphical interpretations and comparisons. FM set includes seven floor records related to ground motions having PGA larger than 0.20 g, and they are considered as a further sub-set of floor records, defined *strong FMs*; they correspond to FM #6,9,15,17,19,21,22. This sub-set was considered for the sake of comparison with GM results since all GMs have PGA larger than 0.20 g. The main details of FMs are reported in Table 2 [48], where PFA and PFV define peak floor acceleration and peak floor velocity, respectively. The mean PFV to PFA (PFA to PGA) ratios related to all FM, FM NF, and FM FF were equal to 0.088, 0.058, and 0.118 s (2.505, 1.891, and 3.235).

Three sets of STPIs were derived from different protocols: (ICC-ES) AC156 [41], FEMA 461 [42], and Wittich and Hutchinson [45] (*Wittich protocol*). Both AC156 and FEMA 461 protocols are intended for generic acceleration-sensitive nonstructural components; AC156 is the only standard explicitly intended for seismic certification purposes, whereas FEMA 461 is among the most authoritative references for seismic assessment and fragility evaluation (seismic qualification). Wittich protocol was developed for freestanding (stiff) components, which typically exhibit a rocking-dominated seismic response.

The procedure developed by Magliulo et al. [53] and used in several other studies [1,14,54] was implemented to generate a set of seven inputs compliant with AC156 protocol (AC156 #1-7). These signals were developed assuming the component location height equal to the building height, corresponding to the most demanding condition. It is worth noting that a recent study [55] suggested that this condition might be associated with non-conservative estimations of the seismic demand on the component due to the limitations provided by the protocol standard for the definition of the required response spectra. Figure 4 shows the time history accelerations related to STPI AC156 set (a_{max} equal to 1.0 g). Three inputs were derived according to FEMA 461 protocol. In particular, FEMA 461 #1 and 2 inputs were directly provided by the protocol standard, whereas input #3 was generated by the authors according to the procedure reported in the FEMA 461 Commentary and referred to the work of Wilcoski et al. [56]. Figure 4 shows the time history accelerations related to STPI FEMA 461 set (a_{max} equal to 1.0 g). It is worth specifying that the reference IM recommended by AC156 protocol is the spectral response acceleration at short periods (S_{DS}), while it corresponds to the spectral ordinate computed at the fundamental period of the component ($Sa(T_C)$) for FEMA 461. a_{max} is considered as an IM in this paper for the sake of generality, as it is often done for incremental analysis of rigid blocks (e.g., [19,27]). In fact, the concept of fundamental period is not consistent for the case of unanchored elements (e.g., for the use of $Sa(T_C)$).

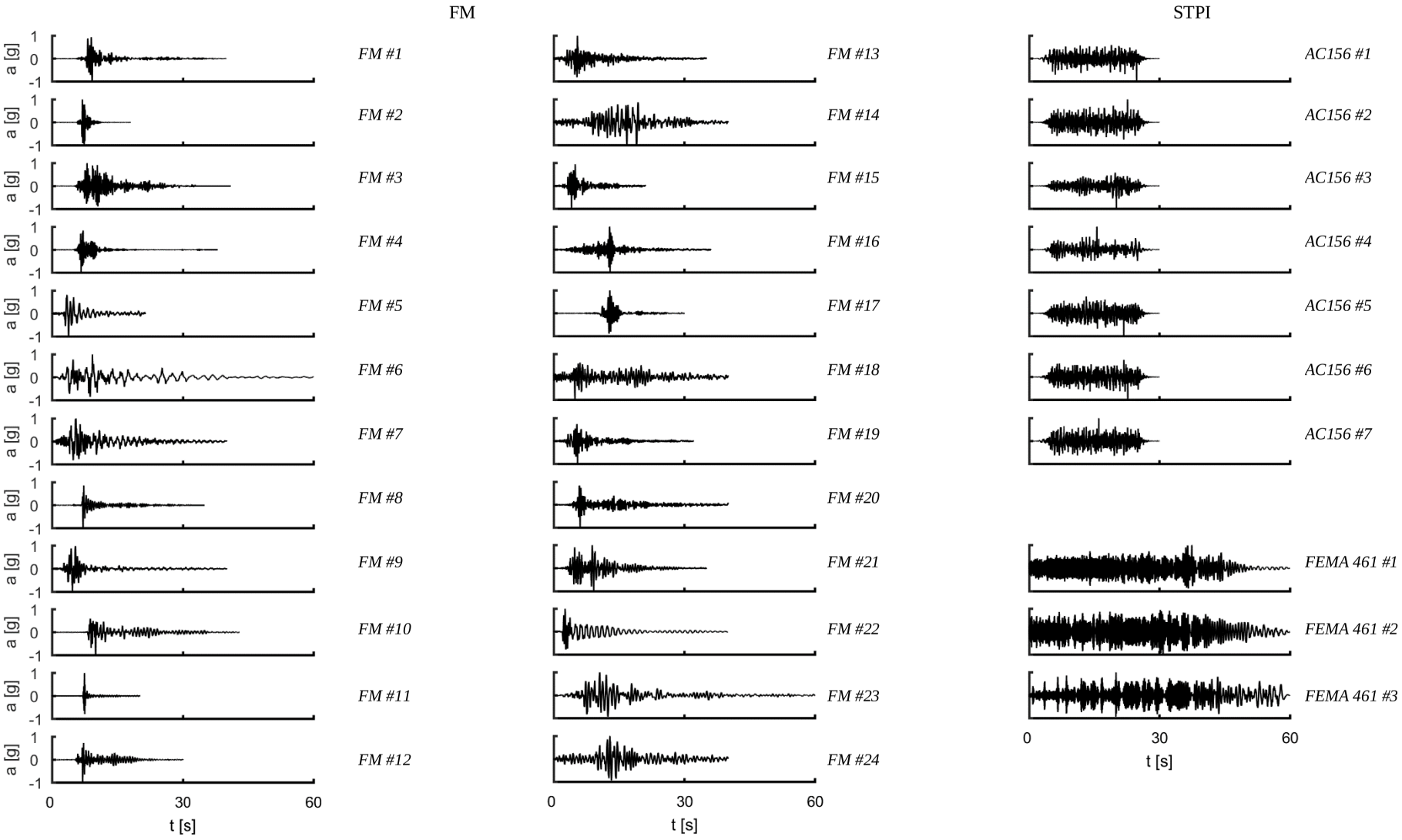

Figure 4: FM and STPI (AC156 and FEMA 461) sets acceleration time histories (a(t)) considering maximum acceleration a_{max} equal to 1.0 g.

Table 2: Main characteristics of the selected FMs [48].

		FM#	Station (building)	Earthquake	Time	Dist [km]	PGA [g]	PGV [m/s]	PFA [g]	PFV [m/s]	$\frac{PGV}{PGA}$ [s]	$\frac{PFA}{PGA}$ [-]
NF	LR	1	Pomona - 2-story Commercial Bldg	Chinohills	29/07/2008 18:42	11.3	0.130	0.116	0.303	0.201	0.091	2.321
		2	Piedmont - 3-story School Office Bldg	Piedmont	20/07/2007 11:42	4.5	0.092	0.041	0.232	0.096	0.046	2.521
		3	Santa Barbara - 3-story UCSB Office Bldg	Islavista	29/05/2013 14:38	7.3	0.083	0.026	0.096	0.042	0.032	1.154
		4	Mammoth Lakes - 1-story High School Gym	MammothLakes	14/12/2016 07:44	3.4	0.071	0.011	0.130	0.033	0.016	1.842
	MR	5	Pomona - 6-story Commercial Bldg	ChinoHills	29/07/2008 18:42	11.5	0.144	0.134	0.384	0.463	0.095	2.669
		6	Van Nuys - 7-story Hotel	Northridge	17/01/1994 12:30	7	0.453	0.509	0.578	0.796	0.115	1.276
		7	Los Angeles - 5-story Warehouse	Whittier87	01/10/1987 14:42	14.3	0.170	0.090	0.234	0.321	0.054	1.378
		8	Van Nuys - 7-story Hotel	Encino	17/03/2014 13:25	9.8	0.145	0.050	0.219	0.104	0.035	1.511
	HR	9	Los Angeles - 8-story CSULA Admin. Bldg.	Whittier87	01/10/1987 14:42	8.4	0.298	0.188	0.462	0.629	0.064	1.549
		10	San Jose - 10-story Residential Bldg	AlumRock	31/10/2007 03:04	14.4	0.114	0.080	0.332	0.172	0.072	2.922
		11	Oakland - 13-story Residential Bldg	berkeley	04/01/2018 10:39	5.3	0.192	0.060	0.367	0.095	0.032	1.909
		12	Oakland - 13-story Residential Bldg	Piedmont	20/07/2007 11:42	6.6	0.056	0.022	0.093	0.039	0.040	1.645
FF	LR	13	Belmont - 2-story Office Bldg	LomaPrieta	18/10/1989 00:04	64.8	0.108	0.128	0.200	0.150	0.120	1.845
		14	Pleasant Hill - 3-story Commercial Bldg	LomaPrieta	18/10/1989 00:04	102.1	0.125	0.214	0.236	0.271	0.174	1.882
		15	Santa Barbara - 3-story UCSB Office Bldg	SantaBarbara	13/08/1978 22:54	81.5	0.270	NA	0.992	0.542	*NA*	3.672
		16	Saratoga - 1-story Gymnasium	MorganHill84	24/04/1984 21:15	29.9	0.100	0.058	0.409	0.182	0.059	4.079
	MR	17	Eureka - 4-story Hospital	Ferndale	10/01/2010 00:27	54.7	0.285	0.301	1.177	0.616	0.108	4.130
		18	Palm Desert - 4-story Office Bldg	PalmSprings86	08/07/1986 09:20	32	0.110	0.087	0.199	0.121	0.080	1.803
		19	Watsonville - 4-story Commercial Bldg	LomaPrieta	18/10/1989 00:04	18.1	0.359	0.549	1.200	0.800	0.156	3.341
		20	Long Beach - 5-story CSULB Engnrng Bldg	Whittier87	01/10/1987 14:42	31.7	0.094	0.061	0.357	0.168	0.067	3.792
	HR	21	Burbank - 10-story Residential Bldg	Northridge	17/01/1994 12:30	21.2	0.301	0.190	0.759	0.633	0.064	2.518
		22	Pasadena - 9-story Commercial Bldg	SierraMadre91	28/06/1991 14:43	18.3	0.246	0.206	0.425	0.419	0.085	1.726
		23	San Jose - 10-story Commercial Bldg	LomaPrieta	18/10/1989 00:04	33.4	0.099	0.213	0.368	0.490	0.219	3.723
		24	Walnut Creek - 10-story Commercial Bldg	LomaPrieta	18/10/1989 00:04	97.9	0.050	0.078	0.242	0.274	0.163	4.916

NF: near-field; FF: far-field; LR: low rise; MR: medium rise; HR: high rise; NA: data not available.

Wittich protocol input is a sinusoidal waveform, and its features depend on the geometry of the component (i.e., component-depending testing input). It is worth recalling that both AC156 and FEMA 461 protocol inputs are not conditioned by the geometry of the component. In particular, the peak frequency of the input should be centered on the frequencies of sensitivity related to the specific component, which can be evaluated considering the free motion of rocking blocks (i.e., rocking frequency f_r) [28,45,46]. Accordingly, the rocking frequency f_r (only) depends on the semi-diagonal dimension of the block (R) and on the initial release angle to critical angle ratio (θ_0/α). A representative input compliant with Wittich protocol is depicted in Figure 5, where acceleration (a) and time (t) are normalized considering a_{max} and duration (dur), respectively. Seven inputs were generated for each block geometry by varying θ_0/α from 0.050 to 0.200, with increments of 0.025. This range was compliant with the typical values assumed in other studies (e.g., [45,57]). A sampling rate equal to 200 Hz was assumed, as a value in between FEMA 461 (100 Hz) and AC156 (400 Hz) rates. The inputs had peak frequencies (durations) ranging within 0.56 – 3.51 Hz (21.8 – 136.3 s).

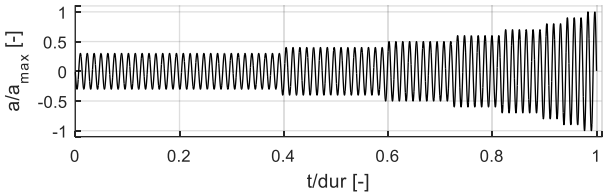

Figure 5: Wittich protocol input acceleration time history with acceleration (a) and time (t) normalized considering maximum acceleration (a_{max}) and the duration (dur), respectively.

Intensity Measures and Damage Conditions

Dimensionless acceleration- and velocity-based IMs were considered for the assessment of the numerical analysis results, i.e., $a_{max}/(g \cdot tan\alpha)$ and $p \cdot v_{max}/(g \cdot tan\alpha)$ [19,27]; $a_{max}/(g \cdot tan\alpha)$ was found to be particularly efficient for rocking onset and overturning assessment of small-to-medium size blocks (e.g., R < 2.0 m), whereas $p \cdot v_{max}/(g \cdot tan\alpha)$ was found to be more efficient for overturning assessment of medium-to-large size blocks (e.g., R > 2.0 m) [19]. These IMs are intensity-based parameters and do not directly account for duration, frequency, and energy, which can play a key role in rocking performance. The reader is referred to [26,43,50] for insights into the potential influence of these IMs. The IM values associated with given $|\theta_{max}/\alpha|$ thresholds can be considered to be IM capacities. As a matter of fact, for a given $|\theta_{max}/\alpha|$ level, the associated IDA IM value represents the IM threshold that defines the exceedance of the $|\theta_{max}/\alpha|$ level by the component in terms of IM; this is associated with an IM capacity of the component.

In this study, the rigid block analyses were performed considering the blocks as directly subjected to the selected loading history sets. In the case of FMs and STPIs, the blocks were meant to be directly excited by real and artificial floor motions, respectively. Therefore, the IM capacities assessed considering the direct analysis results represented the floor response of the blocks. Accordingly, the numerical results, expressed using a_{max} as an IM, represent PFA estimations. These results were processed in order to express the block response in terms of PGA, i.e., accounting for the influence of the building. In particular, relevant PFA to PGA ratios were applied to the PFA results in order to obtain the related PGA values. For FMs, each analysis result (i.e., each IDA datapoint) was processed considering the PFA to PGA ratio related to the specific analysis loading history, as provided by the related database. For STPIs, a constant ratio was assumed for all inputs. This ratio was derived from the set of instrumented RC buildings related to FMs, i.e., the median PFA to PGA ratio (e.g., Table 2). Assessing FM and STPI results by using ground IMs such as $PGA/(g \cdot tan\alpha)$ allows accounting for both acceleration amplification and frequency content filtering actions of the building, whereas using floor IMs such as $a_{max}/(g \cdot tan\alpha)$ only takes into account the frequency content filtering action. For example, comparing the results related to GMs and FMs using $PGA/(g \cdot tan\alpha)$ for the former and $PFA/(g \cdot tan\alpha)$ for the latter evidences the only influence of the building response in terms of frequency content filtering, whereas using $PGA/(g \cdot tan\alpha)$ for both GMs and FMs also accounts for the acceleration amplification action of the building.

$|\theta_{max}/\alpha|$ is defined in the following as dimensionless rocking amplitude. The condition $|\theta_{max}/\alpha| > 0$ determines the rocking motion of the block, and as much as $|\theta_{max}/\alpha|$ increases, the damage is expected to become more significant. Low values of $|\theta_{max}/\alpha|$, e.g., 0.01 to 0.10, are related to rocking onset to low amplitude rocking, which potentially identifies absent to limited damage (e.g., small residual displacements) [19,27]; $|\theta_{max}/\alpha|$ values within 0.20 – 0.40 are related to moderate rocking and possible limited to moderate damage. Larger values are likely to cause more severe damage (e.g., large residual displacements or irreversible component deformation), and $|\theta_{max}/\alpha| \geq 1$ typically corresponds to the overturning of the block (i.e., collapse) [14,58], as it was also assumed in the present study.

SPECTRAL ACCELERATION ANALYSIS

The spectral analysis of real (ground and floor) motions and the definition of compliant design and assessment response spectra is of paramount importance for design and assessment of acceleration-sensitive nonstructural elements [59]. Figure 6, Figure 7, and Figure 8 depict the spectral acceleration Sa versus the period T. In particular, Figure 6 and Figure 7 show the spectra related to real records (GM/FM and NF/FF inputs) and STPI FEMA 461 and AC156 inputs, respectively; Figure 8 depicts the spectra associated with STPI Wittich inputs (for #1C and #2C blocks). The spectra correspond to a_{max} equal to 1.0 g.

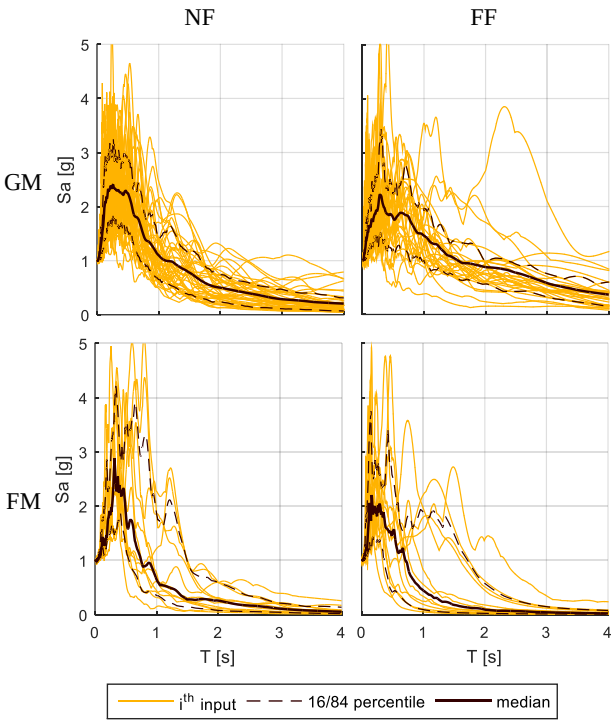

Figure 6: Spectral acceleration Sa versus period T corresponding to real records (GM/FM and NF/FF inputs) considering a_{max} equal to 1.0 g.

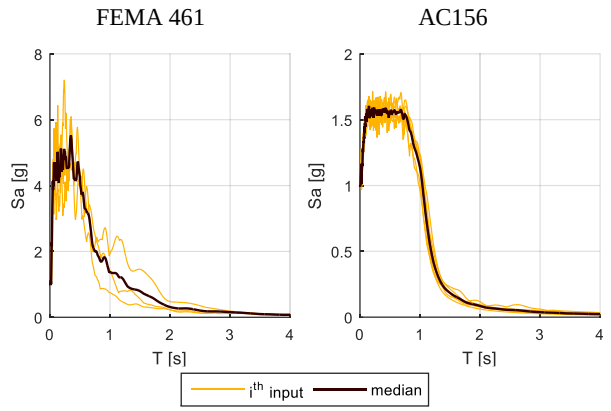

Figure 7: Spectral acceleration Sa versus period T corresponding to STPI AC156 and FEMA 461 inputs considering a_{max} equal to 1.0 g.

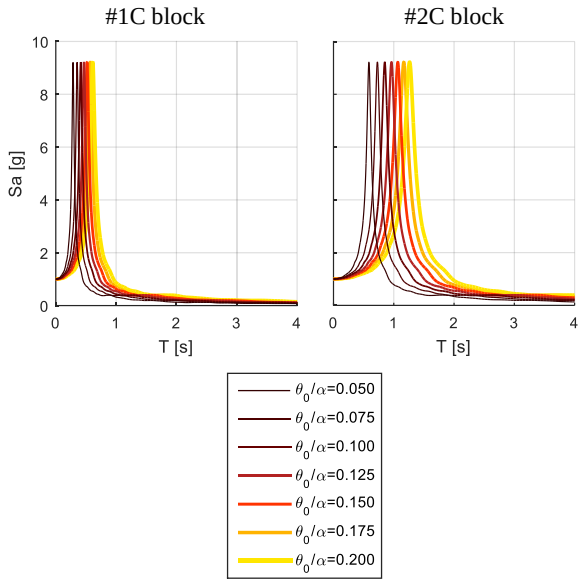

Figure 8: Spectral acceleration Sa versus period T corresponding to STPI Wittich inputs considering a_{max} equal to 1.0 g.

Near-field (and far-field) GMs have more significant frequency contents (i.e., higher spectral ordinate) for lower (and higher) periods, which correspond to periods *T* lower (and higher) than about 0.6 s considering median spectra. A more irregular trend was found regarding FMs: near-field spectra present amplitude peaks higher than far-field ones but the latter have higher frequency amplitudes for very low periods. Moreover, near-field FMs have medium to high period ordinates lower than far-field ones. While the peak amplitude of GMs and FMs are quite similar, the medium to high period ordinates related to GMs are significantly larger than FM ones. FEMA 461 spectra present significantly high peaks and a relatively large scatter despite only three inputs are considered. Conversely, AC156 inputs present relatively reduced accelerations corresponding to the most amplified spectral ordinates (i.e., 1.3-8.3 Hz or 0.12-0.77 s), with very reduced scatter (seven inputs are considered).

Wittich input spectra, shown in Figure 8, have a narrow bell shape with very high acceleration peaks. The variation of θ_0/α affects both the peak period (or frequency) and the width of the bell shape. In particular, the resonant period increases as θ_0/α grows. The magnitude of the increase, in terms of resonant period associated with increasing θ_0/α, becomes more relevant as the block size increases, as it can be observed by comparing #1C and #2C spectra in Figure 8.

Figure 9 shows the spectral acceleration *Sa* versus the frequency *f* instead of the period *T*, as it is typically done for assessment of nonstructural components. In particular, Figure 9.a (b) depicts the spectra related to inputs having a_{max} (PGA) equal to 1.0 g. The inputs related to PGA equal to 1.0 g were obtained by scaling the ones associated with a_{max} equal to 1.0 g according to the procedure reported in the previous section. Figure 9.a highlights the difference among the spectral response of the different input sets only in terms of the frequency contents of the inputs as they are. Conversely, Figure 9.b allows comparing the spectral response also accounting for the considered (building) acceleration amplification.

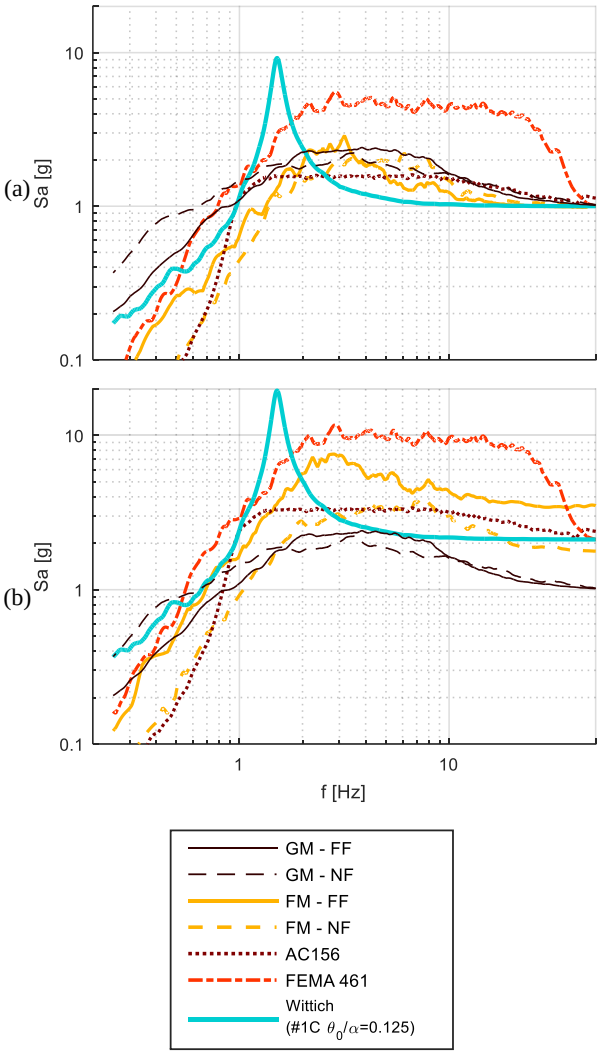

Figure 9: Spectral acceleration Sa versus frequency f for all loading history sets considering (a) a_{max} (or PFA) equal to 1.0 g and (b) PGA equal to 1.0 g.

Considering the only frequency contents (Figure 9.a), GM FF set presents frequency amplitudes significantly higher than FM FF set for low (e.g., $f < 2.0$ Hz) and medium to high frequencies (e.g., $f > 3.5$ - 4 Hz), whereas GM NF set presents frequency amplitudes lower than FM NF set for medium frequencies (e.g., $4.0 < f < 8.5$ Hz). FM FF set exhibits a larger peak amplitude than GM FF set, while the peak response of FM NF set is more comparable to GM NF set one. AC156 inputs have spectral ordinates lower (higher) than FM ones over the most amplified frequencies of FMs (around 1.0 Hz and for medium to large frequencies). Conversely, if the PFA to PGA amplification is also considered (Figure 9.b), FM FF set presents spectral ordinates significantly larger than FM NF set one over the whole frequency range, with peak ordinates that are more

comparable to FEMA 461 ones. AC156 spectral response is never lower than FM NF one, with larger ordinates between 0.8 and 4 Hz and for frequencies higher than 10 Hz. More comments on the spectra are omitted for the sake of brevity since the focus of the work was not on the spectral analysis, and this was functional to the interpretation of the results.

RESULTS AND DISCUSSION

Premise

The numerical results presented in this section are related to more than one thousand IDA curves, which correspond to almost sixty thousand rigid block analyses. The results are presented and discussed in sub-sections considering the most relevant aspects and features: ground and floor motions (discussed both for (set 1) small to medium and (set 2) medium to large size blocks), shake table protocol inputs, and comparisons and key findings. The severity associated with different input sets is meant in terms of estimations of dimensionless IM values (capacities) as a function of dimensionless rocking amplitudes. Regarding a record, the more the dimensionless IM (capacity) estimations associated with given dimensionless rocking amplitudes are small, the more the record is severe. As a matter of fact, a given dimensionless rocking amplitude is reached corresponding to a lower (higher) dimensionless IM (capacity) value under a more (less) severe record. In this study, the overall severity of the different ground and floor input (sub-)sets was quantified through median values of the IDA curves. The 15th and 85th percentile curves were also computed, and the 15th to 85th percentile IM(EDP) range was assessed as a measure of response dispersion.

Ground and Floor Motions

Small to Medium Size Blocks

Figure 10 shows the IDA curves related to real records (GM and FM inputs), corresponding to (set 1) blocks #1A, #1B, #1C, #1D, and #1E; $a_{max}/(g \cdot tan\alpha)$ is used as an IM. GM NF and FF records are associated with quite similar IDA curves in terms of medians (Figure 10 GM), as it was qualitatively found by Petrone et al. [19]. However, the discrepancy between them becomes more sensitive for $R > 1.0$ m blocks and medium to large rocking amplitudes (e.g., $|\theta_{max}/\alpha| > 0.5$), i.e., GM NF records are more severe than GM FF ones (e.g., Figure 10 GM-#1E). FM FF records are significantly more severe than NF ones, especially for $R > 0.5$ m and $|\theta_{max}/\alpha| > 0.2$ (Figure 10 FM-#1B to #1E). Incipient to low amplitude rocking ($0.05 < |\theta_{max}/\alpha| < 0.2$) occurs at very similar a_{max} for both GMs and FMs (Figure 10 GM & FM (medians)), as it was expectable since the rocking initiation phenomenon is significantly more regular than the moderate to severe amplitude rocking [19]. FMs are less severe than GMs for all geometries, especially if NF records are considered (Figure 10 GM & FM (medians)); the discrepancy increases as the block size increases (largest discrepancy corresponding to block #1E). The 15th to 85th percentile range related to GM FF records is quite similar to the NF one (Figure 10 GM). The 15th percentile thresholds related to FF and NF records (Figure 10 FM) approximately coincide, whereas the 85th percentile threshold related to NF records (a) is larger than FF one for blocks #1A, #1B, and #1C, (b) approximately coincides with FF one for block #1D, and (c) is lower than FF one for block #1E. Regarding FM records, the 15th percentile thresholds related to FF and NF records are quite similar, whereas a significant difference is found considering the 85th percentile threshold (Figure 10 FM). In particular, the FF record threshold is significantly lower than NF one, especially for R < 1.50 m blocks. The 15th to 85th percentile range related to GM is significantly smaller than FM one (Figure 10 GM and Figure 10 FM), and most of the discrepancy is due to the 85th percentile thresholds (the 15th percentile thresholds related to FM FF and NF are quite similar).

Figure 11 shows the median IDA curves for set 1 blocks considering real records (GM and FM inputs) and using $PGA/(g \cdot tan\alpha)$ and $PFA/(g \cdot tan\alpha)$ as IMs. The influence of the block size on the IDA curves is less significant for GM records (and $PGA/(g \cdot tan\alpha)$), whereas this is quite significant for FM ones using $PGA/(g \cdot tan\alpha)$, especially for smaller blocks. As a matter of fact, the IDA curves related to blocks #1A ($R = 0.36$ m) and #1B/C/D ($R = 0.72$ m) are overall more similar among them than ones associated with the blocks #1B/C/D ($R = 0.72$ m) and #1E ($R = 1.43$ m) (Figure 11). FM FF inputs are significantly more severe than GM ones, whereas FM NF inputs are more severe than GM NF records only for small to medium rocking amplitudes (e.g., $|\theta_{max}/\alpha| < 0.4$). If large to overturning rocking is considered, only FM NF inputs related to the smallest block size are more severe than GM NF ones. The influence of the geometry on FM IDA curves considering $PFA/(g \cdot tan\alpha)$ was already discussed with regard to Figure 10; however, this has a trend similar to Figure 11 FM (using $PGA/(g \cdot tan\alpha)$).

A clear trend can be identified considering the damage severity associated with the block size, especially considering FMsThe component damage decreases as the block size increases (i.e., throughout blocks #1A, 1C, and 1E) for a given level of dimensionless acceleration, as it was established in the literature (e.g., [6]). The influence of the block slenderness is less relevant, as it can be seen by comparing the results related to blocks #1B, 1C, and 1D (e.g., Figure 11 FM using $PFA/(g \cdot tan\alpha)$). It is recalled that dimensionless IMs were considered and $tan\alpha$ was used to obtain them. Therefore, the effect of the slenderness variability was already expected to be not particularly significant (e.g., [27,60]). Only a (minor) anomaly is found, and this is related to the case of block #1C and FM NF, which exhibited higher intensity thresholds over $0.35 < |\theta_{max}/\alpha| < 0.65$ if compared to the blocks having the same size and different slenderness (i.e., #1B and 1D), as it can be seen in Figure 11 FM using $PGA/(g \cdot tan\alpha)$ and Figure 11 FM using $PFA/(g \cdot tan\alpha)$. It is worth mentioning that the role played by both size and slenderness of the blocks is typically not straightforward and that the combined effect of them can be quite complex (e.g., [6]), especially if earthquake records are considered instead of sinusoidal or theoretical-based loading histories [34,38]. Therefore, the mentioned trends cannot be easily generalized, especially regarding the slenderness.

Medium to Large Size Blocks

Figure 12 shows the IDA curves related to real records (GM and FM inputs), corresponding to (set 2) blocks #2A, #2B, #2C, #2D, and #2E; $p \cdot v_{max}/(g \cdot tan\alpha)$ is used as an IM. GM FF records have a severity similar to GM NF ones in terms of median (Figure 12 GM). The 15th percentile thresholds related to (GM) FF and NF records are approximately coinciding for all blocks but #2A (Figure 12 GM-#2A), whereas the 85th percentile threshold related to FF records is overall lower than NF one, except for block #2E (Figure 12 GM-#2E). FM FF records are overall more severe than FM NF ones (Figure 12 FM), especially for R > 1.0 m blocks (Figure 12 FM-#2B to Figure 12 FM-#2E). Overall, FM FF median IDA is slightly less severe than GM FF one (Figure 12 GM & FM (medians)), and the discrepancy is more significant, but still minor, only for severe to overturning rocking amplitudes.

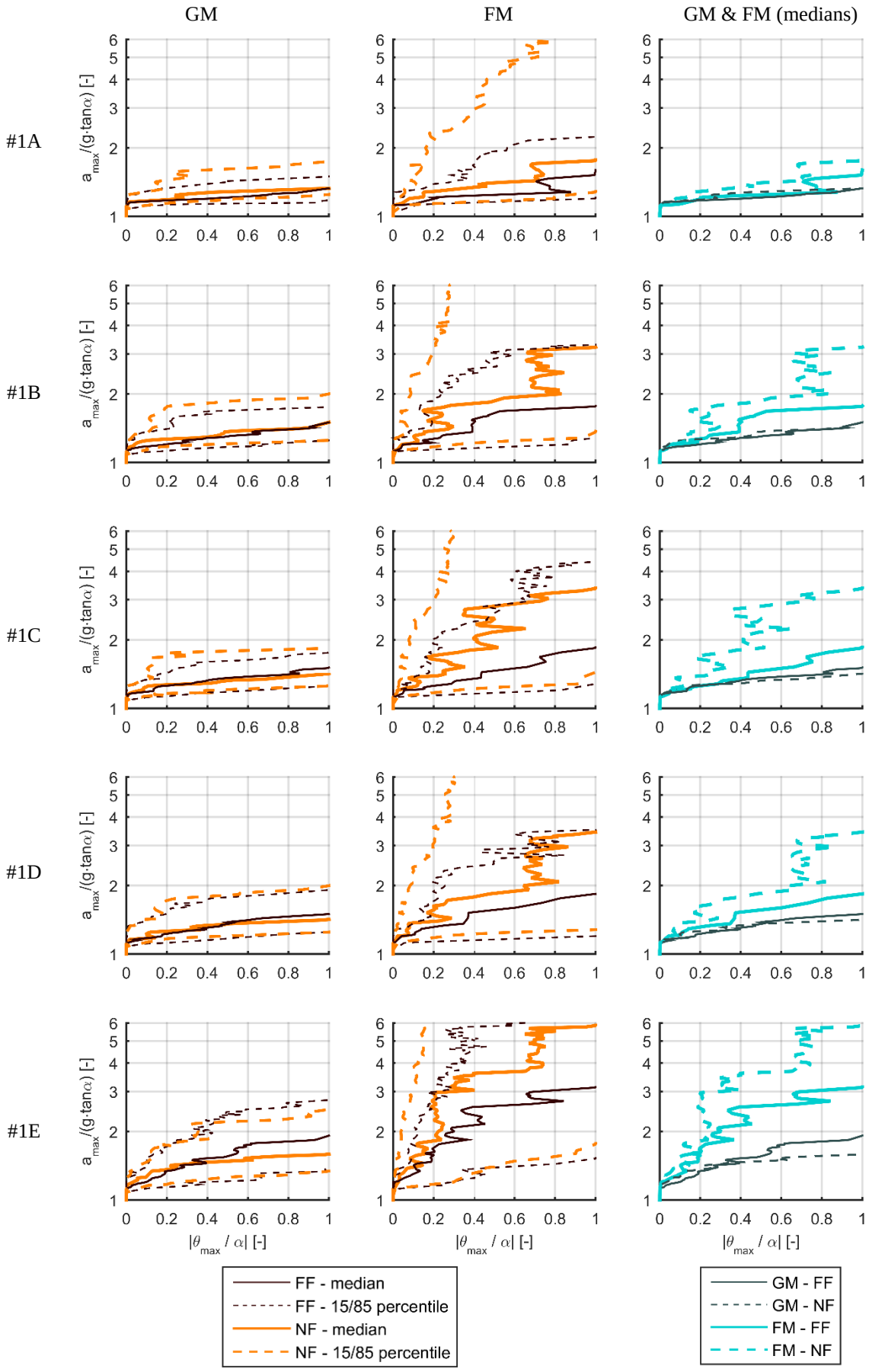

Figure 10: IDA curves corresponding to real records (GM and FM inputs) using $a_{max}/(g \cdot \tan\alpha)$ as an IM; a_{max} corresponds to PGA (PFA) for GMs (FMs).

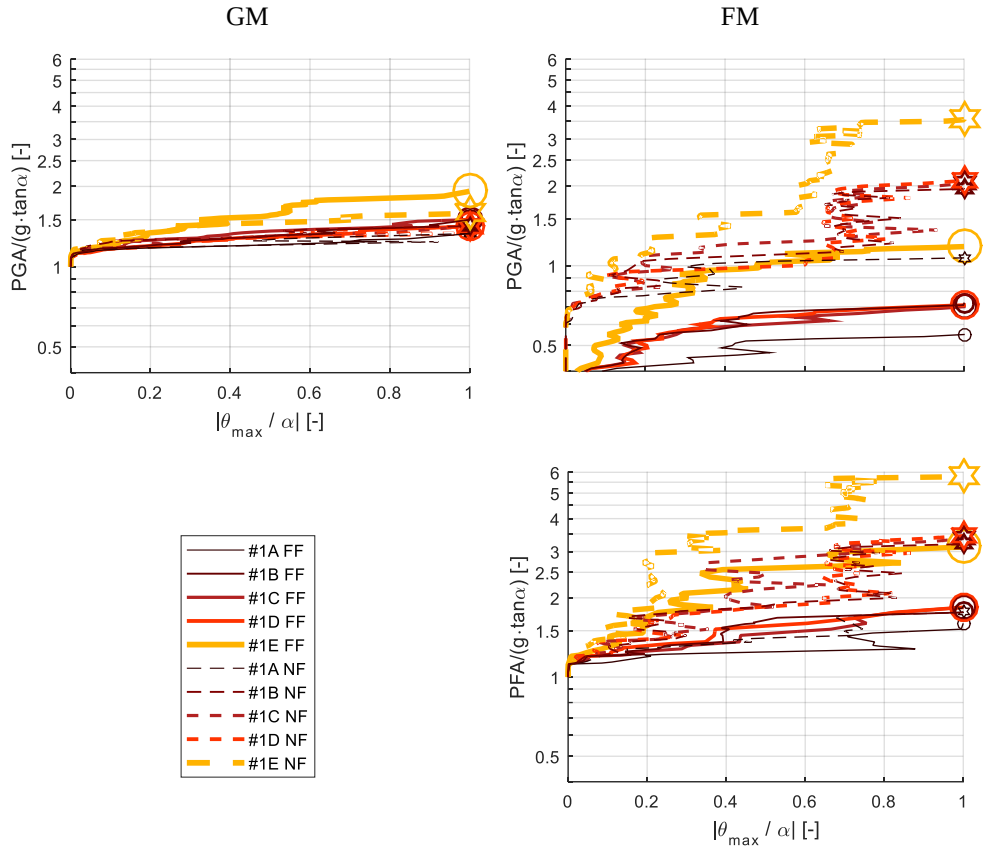

Figure 11: Median IDA curves for set 1 blocks corresponding to real records (GM an FM inputs) using PGA/(g·tanα) and PFA/(g·tanα) as IMs.

Conversely, FM NF inputs are significantly less severe than GMs for medium to large rocking amplitudes (and larger blocks), similarly to the case related to set 1 blocks and $a_{max}/(g \cdot tan\alpha)$. The 15th to 85th percentile range is relatively comparable for GM FF and NF records (Figure 12 GM). In particular, the 15th percentile threshold is quite similar for FF and NF records, whereas the 85th percentile one related to FF is slightly lower than NF one.

A different trend is noted regarding FM records. In particular, the 15th to 85th percentile range related to FM FF records is significantly smaller than the FM NF one (Figure 12 FM-#2A): a large difference is observed between the 85th percentile thresholds, whereas the 15th percentile thresholds are more similar. GM records present an 85th percentile threshold that is significantly lower than FM ones (Figure 12 GM and Figure 12 FM), whereas the 15th percentile thresholds related to GM and FM are more comparable, similarly to the case of set 1 blocks and $a_{max}/(g \cdot tan\alpha)$. The 15th to 85th percentile range related to GM is significantly smaller than FM one (Figure 10 GM and Figure 10 FM), and most of the discrepancy is due to the 85th percentile thresholds (the 15th percentile thresholds related to GM and FM are quite similar). The significantly large 85th percentile threshold associated with FM NF records is due to several FM NF records that determine very reduced rocking amplitudes under a significantly high $p \cdot PFV/(g \cdot tan\alpha)$ values. For these records, the IDA curves exhibit a linear behavior over minor to moderate rocking amplitudes, with significant irregularity and scatter.

Figure 13 shows the median IDA curves for set 2 blocks considering real records (GM and FM inputs) and using $p \cdot PGV/(g \cdot tan\alpha)$ and $p \cdot PFV/(g \cdot tan\alpha)$ are used as IMs. The scatter of the (median) IDA curves is not as significant as it is for set 1 blocks and $PGA/(g \cdot tan\alpha)$ and $PFA/(g \cdot tan\alpha)$, especially if the former IM is considered. FM FF records are particularly more severe than GM FF ones if $PGA/(g \cdot tan\alpha)$ is considered as an IM, whereas FM NF inputs are less severe than GM NF ones for all blocks but the smallest (#2A), except in the case of small rocking amplitudes ($|\theta_{max}/\alpha| < 0.3$-$0.4$), where an opposite trend is observed, even if with less significant magnitude.

The trend between the damage severity and the block geometry (size and slenderness) is similar to the case related to $PGA/(g \cdot tan\alpha)$ and $PFA/(g \cdot tan\alpha)$, shown in Figure 11. Only two (minor) anomalies are observed with regard to FMs. (1) Considering $p \cdot PFV/(g \cdot tan\alpha)$, block #2B is associated with higher intensity thresholds over $|\theta_{max}/\alpha| > 0.75$ if compared to blocks #2C and 2D. (2) Blocks #2B, 2C, and 2D exhibit a different damage trend regarding the slenderness if FF $p \cdot PGV/(g \cdot tan\alpha)$ and $p \cdot PFV/(g \cdot tan\alpha)$ results are compared. However, the discrepancies are minor if the differences identified with blocks #2A and #2E are considered as a reference. These anomalies regarding the influence of size and slenderness on component damage stress the heavy nonlinearity of the rocking motion and the significance of the record-to-record variability.

Shake Table Protocol Inputs

Figure 14 shows the IDA curves for set 1 blocks using $PFA/(g \cdot tan\alpha)$ and set 2 blocks using $p \cdot PFV/(g \cdot tan\alpha)$, corresponding to STPIs (AC156, FEMA 461, and Wittich). Considering set 1 blocks together with $PFA/(g \cdot tan\alpha)$, AC156 inputs are particularly mild if compared with both FEMA 461 and Wittich ones, especially for larger blocks. The influence of the block size on the IDA curves is clearer and more significant for AC156 than for the other cases, especially considering larger rocking amplitudes ($|\theta_{max}/\alpha| > 0.3$-$0.4$). Overall, the slenderness does not have a significant effect on the IDA curves for all protocol sets.

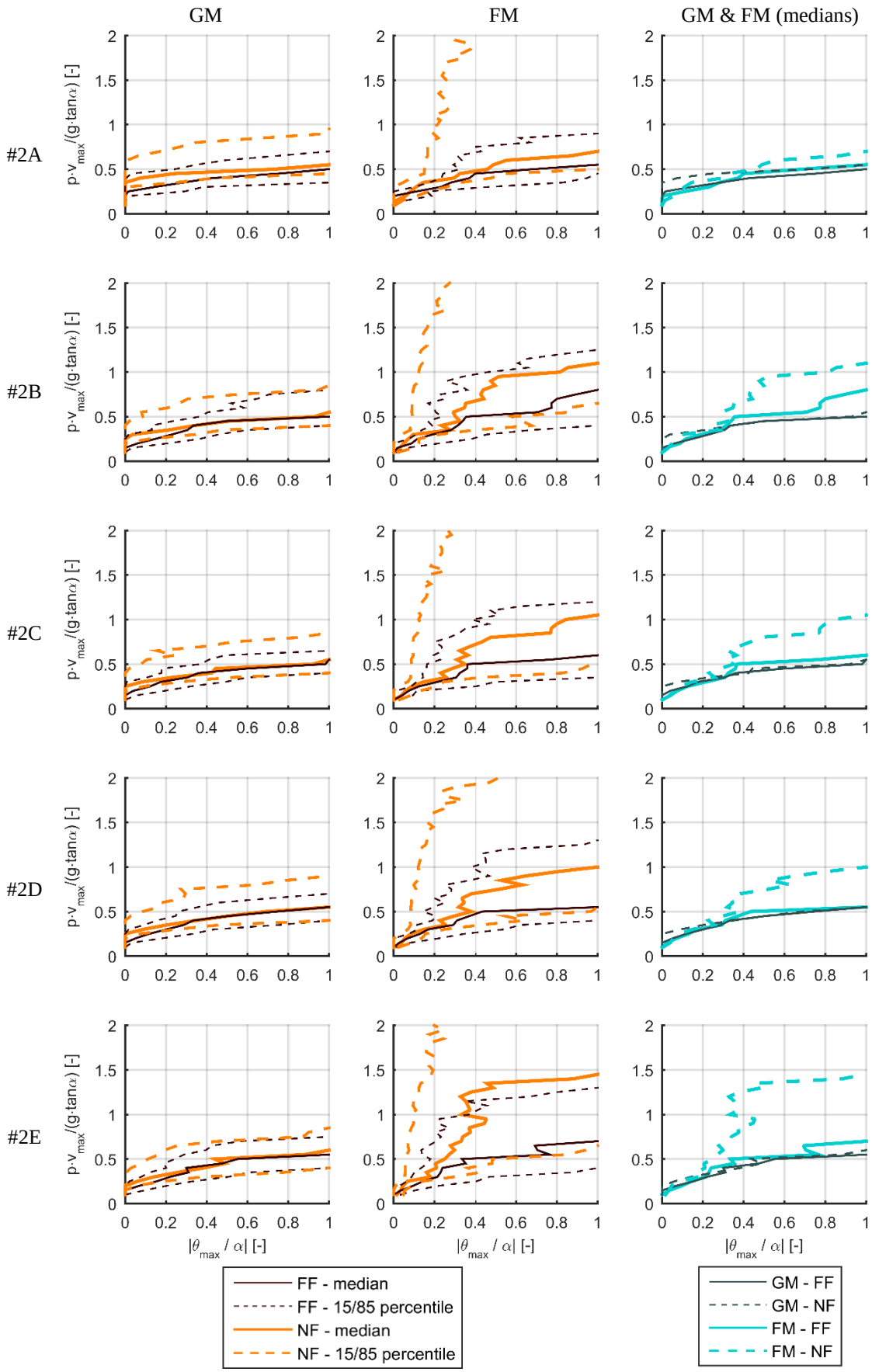

Figure 12: IDA curves corresponding to real records (GM and FM inputs) using $a_{max}/(g \cdot \tan\alpha)$ as an IM; a_{max} corresponds to PGA (PFA) for GMs (FMs).

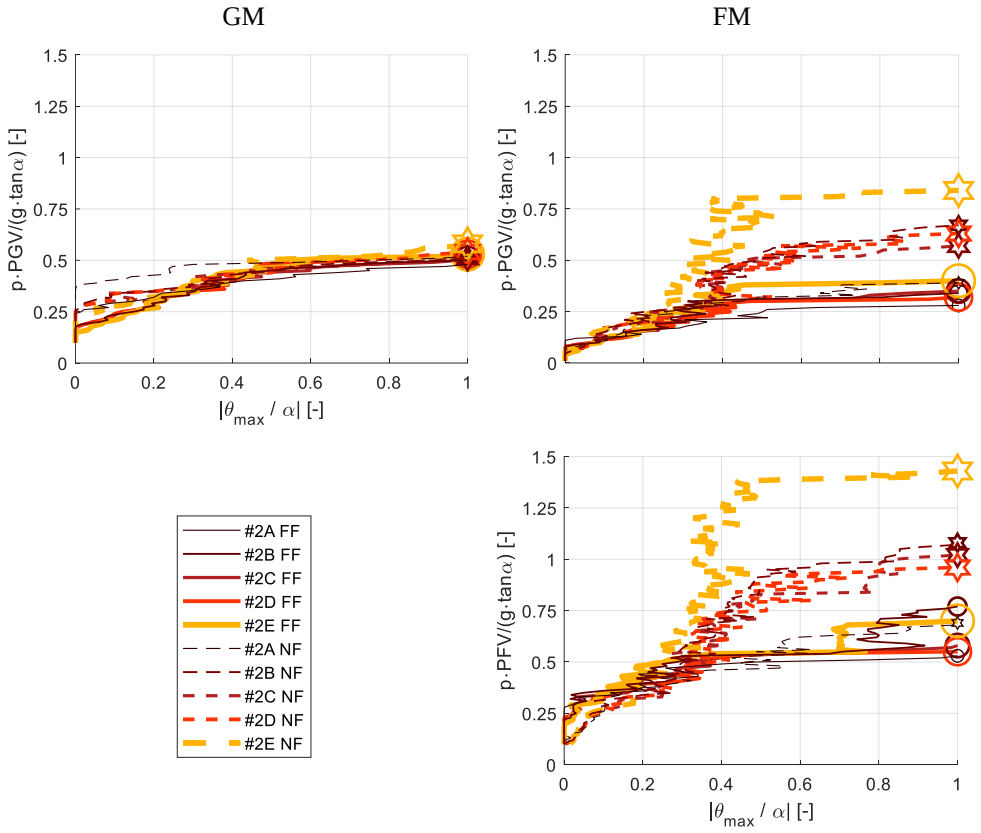

Figure 13: Median IDA curves corresponding to real records (GM and FM inputs) using p·PGV/(g·tanα) and p·PFV/(g·tanα) as an IM.

For FEMA 461, all curves but block #1E one are quite similar among them, and minor discrepancies are found only for large amplitudes ($|\theta_{max}/\alpha| > 0.6$). Wittich results do not show a significant scatter due to different block size or slenderness, and all block curves are essentially coincident over the whole amplitude range. It is worth noting that Wittich protocol inputs are particularly severe for small to medium rocking amplitudes ($|\theta_{max}/\alpha| < 0.5$), whereas they produce IDA curves quite similar to FEMA 461 for larger amplitudes, except for block #1E. In particular, for FEMA 461, this block is associated with significantly larger accelerations over $|\theta_{max}/\alpha| > 0.4$ rocking amplitudes. AC156 inputs are significantly less severe than the other ones over the whole rocking amplitude range.

The trends of the block size and slenderness versus IDA severity related to set 2 blocks and *p·PFV/(g·tanα)* are similar to the ones related to set 1 blocks and *PFA/(g·tanα)*, even though two anomalies can be identified. (1) Block #2B and AC156 results: the exhibited motion is quite similar to or larger than the one related to the block #2E for medium to large amplitudes ($|\theta_{max}/\alpha| > 0.4$). (2) Block #2E and Wittich results: the accelerations are lower than all other (large) blocks for medium to large rocking amplitudes ($|\theta_{max}/\alpha| > 0.5$). Except for medium rocking amplitudes ($0.3 < |\theta_{max}/\alpha| < 0.7$), AC156 and FEMA 461 produce similar IDA curves even though AC156 results are more dispersed and irregular. Wittich results do not present a significant scatter due to the different geometries, and the inputs are particularly less severe than the other set ones for small amplitudes ($|\theta_{max}/\alpha| < 0.3$), while their response is quite similar to the ones related to AC156 medium to large blocks.

The rocking amplitude corresponding to $0.8 – 0.9 \leq |\theta_{max}/\alpha| < 1$ (severe rocking) did present very few data points (i.e., incremental step results) if compared to other motion ranges, especially considering the protocol inputs. Such motion range is particularly unstable with regard to the overturning and reaching this condition (i.e., $|\theta_{max}/\alpha| > 0.8 – 0.9$) might also represent a sufficient condition for block overturning when the blocks are subjected to the protocol inputs. In other words, this might suggest that once a relatively critical normalized rotation $|\theta_{max}/\alpha|$ is reached, the blocks hardly keep experiencing rocking response without overturning, and the IM threshold associated with reaching this critical normalized rotation is critically close to the one corresponding to the overturning.

Comparisons and Key Findings

A comparison among the median IDA curves related to the different input sets is depicted in Figure 15, where representative blocks (i.e., #1C and #2C) are considered as a reference; it is recalled that blocks #1C and #2C are representative of building contents (a hospital cabinet) and monumental elements (a Greek temple column). Considering block #1C, Wittich, FEMA 461, and GM sets produce very similar IDA curves over the whole rocking amplitude range, and Wittich (FEMA 461) inputs are the most severe for low to moderate (severe rocking amplitude to overturning) rocking amplitudes, i.e., $|\theta_{max}/\alpha| \leq 0.60$ ($|\theta_{max}/\alpha| \geq 0.60$). For low to moderate rocking amplitudes, AC156 inputs are significantly less severe than FM FF, whereas the former and the latter produce quite similar IDA curves for severe rocking amplitudes ($|\theta_{max}/\alpha| \geq 0.70$). AC156 inputs are less severe than FM NF only for low rocking amplitudes ($|\theta_{max}/\alpha| \leq 0.30$), while FM NF inputs are relatively mild over moderate rocking amplitude to overturning. The trend of severity of the different sets is more complex and irregular for block #2C and using *p·PFV/(g·tanα)*. It is recalled that *PFA/(g·tanα)* was found to be more efficient than *p·PFV/(g·tanα)* for rocking onset ($|\theta_{max}/\alpha| = \sim 0$) even for medium to large size blocks by Petrone et al. [19], while the latter IM was found to be more efficient regarding overturning ($|\theta_{max}/\alpha| = 1$).

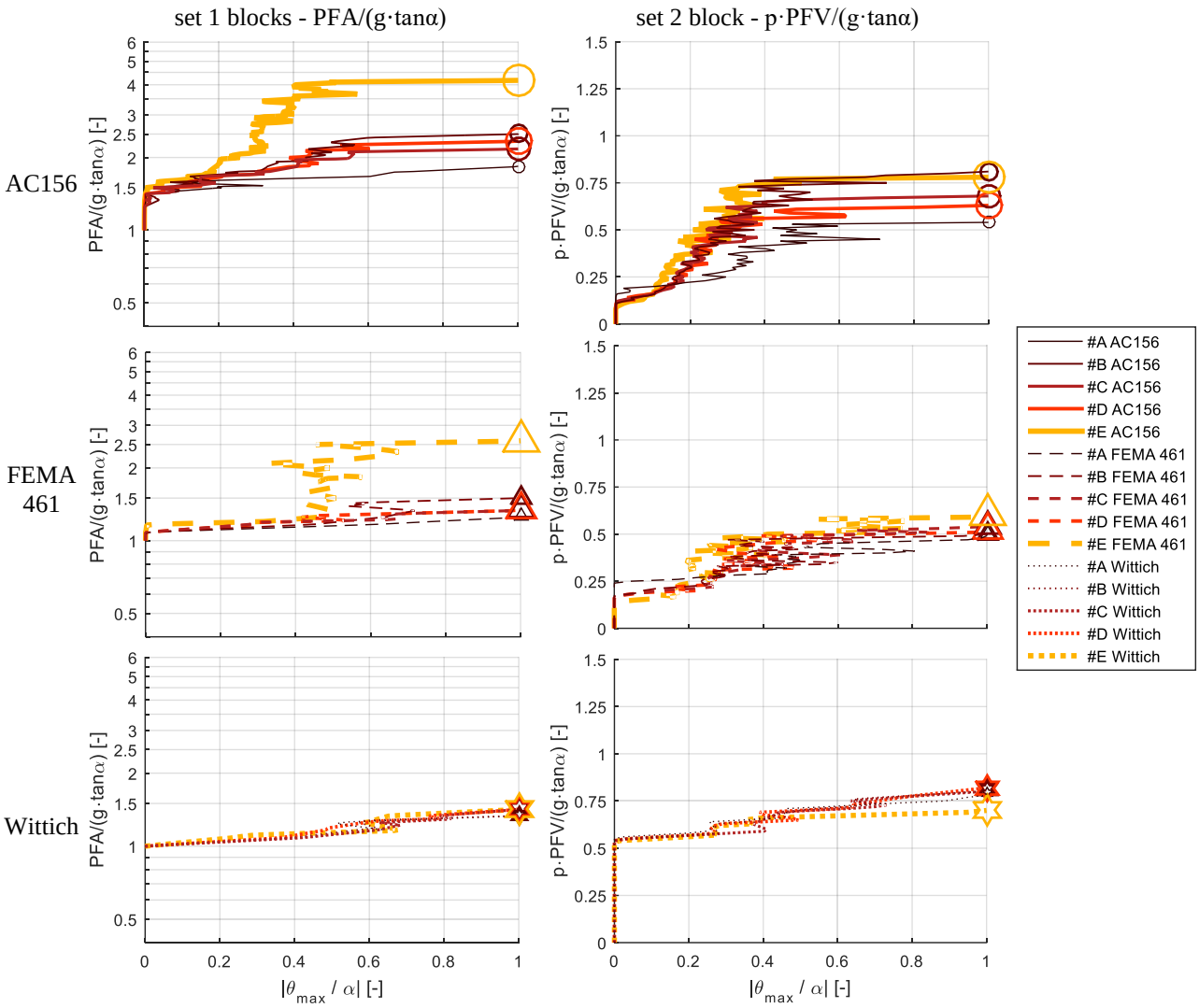

Figure 14: Median IDA curves corresponding to STPIs (AC156, FEMA 461, and Wittich).

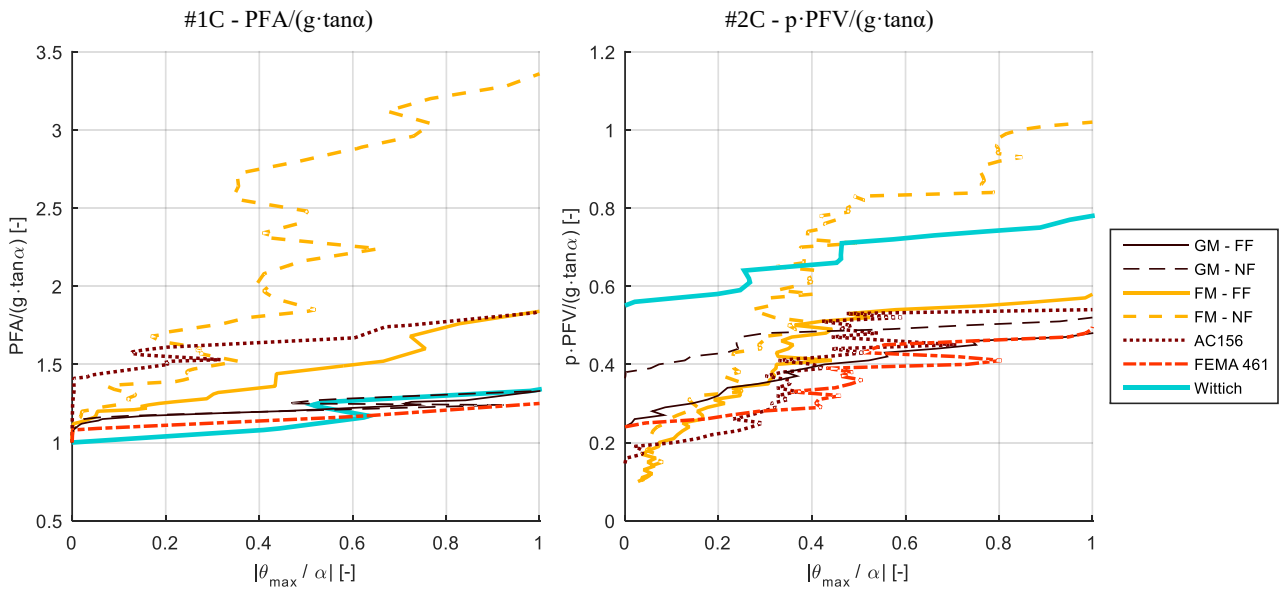

Figure 15: Comparison among all median IDA curves related to blocks #1C and #2C, using PFA/(g·tanα) and p·PFV/(g·tanα), respectively.

No information is available in the literature on the efficiency of such IMs regarding rocking responses other than rocking onset and overturning damage states, i.e., for ~0 < $|\theta_{max}/\alpha|$ < 1. However, the assessment efficiency of the IMs regarding the rocking response of blocks is not the objective of this study. Therefore, the focus of the present comparison is on the moderate rocking to overturning amplitude damage, given the prospective efficiency of the considered IM.

Differently from the case of block #1C together with *PFA/(g·tanα)*, Wittich inputs are particularly mild considering block #2C together with *p·PFV/(g·tanα)*, and only for moderate rocking amplitude to overturning ($|\theta_{max}/\alpha| \geq 0.60$), another set is less severe (i.e., FM NF). The other sets produce similar results; FEMA 461 inputs are the most severe for $|\theta_{max}/\alpha| \geq 0.30$, with IDA curves quite similar to GM NF ones for moderate rocking amplitude to overturning ($|\theta_{max}/\alpha| \geq 0.50$). AC156 inputs produce IDA curves that are very similar to FM FF ones. Differently from the case of of block #1C and *PFA/(g·tanα)*, GM NF and GM FF IDA curves are sensibly different, stressing the differences in terms of velocity to acceleration ratios related to the different sets.

CONCLUSIONS

The paper investigated the rocking response of unanchored acceleration-sensitive structural and nonstructural components subjected to various loading histories, including real ground and floor motions and shake table protocol inputs. The key findings of the study are summarized in the following.

1. FEMA 461 protocol spectra have ordinates significantly larger than AC156 ones when the loading histories are expressed considering the same peak acceleration and present larger scatter despite the lower number of considered inputs (i.e., three FEMA 461 inputs and seven AC156 ones).
2. The resonant period related to Wittich protocol inputs increases as the initial release angle to critical angle ratio (θ_0/α) grows, with magnitude that is increasing as the block size grows.
3. Considering dimensionless peak floor accelerations (PFA) and small to medium size blocks (R < 1.50 m; R is semi-diagonal block dimension), FEMA 461 and Wittich protocols produce (intensity measure (IM)) capacities compatible with ground motions over the whole rocking amplitude range, whereas AC156 inputs are more compatible with far-field floor motions, often determining larger (IM) capacities. Near-field floor motions produce significantly large capacities, especially for medium to large rocking amplitudes.
4. Considering dimensionless peak floor velocities (PFV) and medium to large blocks (R > 1.50 m), FEMA 461 and AC156 protocols are more compatible with far-field ground and floor motions, whereas Wittich input determine the largest capacities (over the whole rocking amplitude range) except for medium to large rocking spectra, where near-field floor motions produce the largest estimations. Near-field ground motions are associated with (a) relatively large capacities for small rocking amplitudes and (b) capacities between FEMA 461-far-field ground motions and AC156-far-field floor motions.
5. Floor motions present a response dispersion larger than ground motions considering both dimensionless acceleration and velocity peak intensity measures, and this is primarily due to the upper percentile thresholds (e.g., 85th percentile). Near-field floor motions present a significantly large dispersion if compared with far-field floor motions and both far- and near-field ground motions.

The developed IDA curves can be considered as a reference for expeditious rocking/overturning assessment. For example, the median and 15th/85th percentile IM capacity associated with specific dimensionless amplitude thresholds (e.g., unitary value for the overturning assessment) can be estimated for geometries compatible with the investigated ones and considering the record set of interest.

Further studies should be performed focusing on the quantitative influence of the building response, also providing fragility and vulnerability estimations.

ACKNOWLEDGEMENTS

The research study presented in this paper was supported by the Italian Department of Civil Protection in the framework of the national project DPC-ReLUIS 2019-2021 “Code contributions for nonstructural elements”.

REFERENCES

1. Cosenza E, Di Sarno L, Maddaloni G, Magliulo G, Petrone C and Prota A (2015). “Shake table tests for the seismic fragility evaluation of hospital rooms”. *Earthquake Engineering and Structural Dynamics*, **44**(1): 23–40. https://doi.org/10.1002/eqe.2456
2. Perrone D, Calvi PM, Nascimbene R, Fischer EC and Magliulo G (2019). “Seismic performance of non-structural elements during the 2016 Central Italy earthquake”. *Bulletin of Earthquake Engineering*, **17**(10): 5655–5677. https://doi.org/10.1007/s10518-018-0361-5
3. Filiatrault A, Perrone D, Merino RJ and Calvi GM (2018). “Performance-based seismic design of nonstructural building elements”. *Journal of Earthquake Engineering*, **25**(2): 237-269. https://doi.org/10.1080/13632469.2018.1512910
4. Anooshehpoor A and Brune JN (2002). “Verification of precarious rock methodology using shake table tests of rock models”. *Soil Dynamics and Earthquake Engineering*, **22**(9–12): 917–922. https://doi.org/10.1016/S0267-7261(02)00115-X
5. Purvance MD, Anooshehpoor A and Brune JN (2008). “Freestanding block overturning fragilities: Numerical simulation and experimental validation”. *Earthquake Engineering and Structural Dynamics*, **37**(5): 791–808. https://doi.org/10.1002/eqe.789
6. Makris N and Kampas G (2016). “Size versus slenderness: Two competing parameters in the seismic stability of free-standing rocking columns”. *Bulletin of the Seismological Society of America*, **106**(1): 104–122. https://doi.org/10.1785/0120150138
7. Konstantinidis D and Makris N (2005). “Seismic response analysis of multidrum classical columns”. *Earthquake Engineering and Structural Dynamics*, **34**(10): 1243–1270. https://doi.org/10.1002/eqe.478
8. Drosos V and Anastasopoulos I (2014). “Shaking table testing of multidrum columns and portals”. *Earthquake Engineering and Structural Dynamics*, **43**(11): 1703–1723. https://doi.org/10.1002/eqe.2418
9. Gesualdo A, Iannuzzo A, Monaco M and Penta F (2018). “Rocking of a rigid block freestanding on a flat pedestal”. *Journal of Zhejiang University-SCIENCE A*, **19**(5): 331–345. https://doi.org/10.1631/jzus.A1700061
10. Jaimes MA, Chávez MM, Peña F and García-Soto AD (2021). “Out-of-plane mechanism in the seismic risk of masonry façades”. *Bulletin of Earthquake Engineering*, **19**(3): 1509–1535. https://doi.org/110.1007/s10518-020-01029-1

11. Agalianos A, Psychari A, Vassiliou MF, Stojadinovic B and Anastasopoulos I (2017). "Comparative assessment of two rocking isolation techniques for a motorway overpass bridge". *Frontiers in Built Environment*, **3**: 47. https://doi.org/110.3389/fbuil.2017.00047
12. Zhang J, Xie Y and Wu G (2019). "Seismic responses of bridges with rocking column-foundation: A dimensionless regression analysis". *Earthquake Engineering and Structural Dynamics*, **48**(1): 152–170. https://doi.org/110.1002/eqe.3129
13. Kelly TE (2009). "Tentative seismic design guidelines for rocking structures". *Bulletin of the New Zealand Society for Earthquake Engineering*, **42**(4): 239–274. https://doi.org/110.5459/bnzsee.42.4.239-274
14. Di Sarno L, Magliulo G, D'Angela D and Cosenza E (2019). "Experimental assessment of the seismic performance of hospital cabinets using shake table testing". *Earthquake Engineering and Structural Dynamics*, **48**(1): 103–123. https://doi.org/110.1002/eqe.3127
15. Konstantinidis D and Makris N (2009). "Experimental and analytical studies on the response of freestanding laboratory equipment to earthquake shaking". *Earthquake Engineering and Structural Dynamics*, **38**(6): 827–848. https://doi.org/110.1002/eqe.871
16. Ebad Sichani M, Padgett JE and Bisadi V (2018). "Probabilistic seismic analysis of concrete dry cask structures". *Structural Safety*, **73**: 87–98. https://doi.org/10.1016/j.strusafe.2018.03.001
17. Dar A, Konstantinidis D and El-Dakhakhni WW (2016). "Evaluation of ASCE 43-05 seismic design criteria for rocking objects in nuclear facilities". *Journal of Structural Engineering*, **142**(11): 04016110. https://doi.org/10.1061/(ASCE)ST.1943-541X.0001581
18. Fragiadakis M and Diamantopoulos S (2020). "Fragility and risk assessment of freestanding building contents". *Earthquake Engineering and Structural Dynamics*, **49**(10): 1028–1048. https://doi.org/10.1002/eqe.3276
19. Petrone C, Di Sarno L, Magliulo G and Cosenza E (2017). "Numerical modelling and fragility assessment of typical freestanding building contents". *Bulletin of Earthquake Engineering*, **15**(4): 1609–1633. https://doi.org/10.1007/s10518-016-0034-1
20. Jaimes MA, Reinoso E and Esteva L (2013). "Seismic vulnerability of building contents for a given occupancy due to multiple failure modes". *Journal of Earthquake Engineering*, **17**(5): 658–672. https://doi.org/10.1080/13632469.2013.771588
21. Masi A, Santarsiero G, Gallipoli MR, Mucciarelli M, Manfredi V, Dusi A and Stabile TA (2014). "Performance of the health facilities during the 2012 Emilia (Italy) earthquake and analysis of the Mirandola hospital case study". *Bulletin of Earthquake Engineering*, **12**(5): 2419–2443. https://doi.org/10.1007/s10518-013-9518-4
22. Mieler MW, Uma SR and Mitrani-Reiser J (2016). "Using failure analysis tools to establish seismic resilience objectives for building components and systems". *Bulletin of the New Zealand Society for Earthquake Engineering*, **49**(1): 86–97. https://doi.org/10.5459/bnzsee.49.1.86-97
23 Rashid M, Dhakal RP and Sullivan TJ (2021). "Seismic design of acceleration-sensitive non-structural elements in New Zealand: State-of-practice and recommended changes". *Bulletin of the New Zealand Society for Earthquake Engineering*, **54**(4): 243-262. https://doi.org/10.5459/bnzsee.54.4.243-262
24. Sorrentino L, Liberatore L, Decanini LD and Liberatore D (2014). "The performance of churches in the 2012 Emilia earthquakes". *Bulletin of Earthquake Engineering*, **12**(5): 2299–2331. https://doi.org/10.1007/s10518-013-9519-3
25. Bakhtiary E and Gardoni P (2016). "Probabilistic seismic demand model and fragility estimates for rocking symmetric blocks". *Engineering Structures*, **114**: 25–34. https://doi.org/10.1016/j.engstruct.2016.01.050
26. Shenton III HW and Jones NP (1991). "Base excitation of rigid bodies. I: Formulation". *Journal of Engineering Mechanics*, **117**(10): 2286–2306. https://doi.org/10.1061/(ASCE)0733-9399(1991)117:10(2286)
27. Dimitrakopoulos EG and Paraskeva TS (2015). "Dimensionless fragility curves for rocking response to near-fault excitations". *Earthquake Engineering and Structural Dynamics*, **44**(12): 2015–2033. https://doi.org/10.1002/eqe.2571
28. Housner GW (1963). "The behavior of inverted pendulum structures during earthquakes". *Bulletin of the Seismological Society of America*, **53**(2): 403–417. https://doi.org/10.1785/BSSA0530020403
29. Yim CS, Chopra AK and Penzien J (1980). "Rocking response of rigid blocks to earthquakes". *Earthquake Engineering and Structural Dynamics*, **8**(6): 565–587. https://doi.org/10.1002/eqe.4290080606
30. Aslam M, Scalise DT and Godden WG (1980). "Earthquake rocking response of rigid blocks". *Journal of the Structural Division*, **106**(2): 377-392. https://cedb.asce.org/CEDBsearch/record.jsp?dockey=0009293
31. Ishiyama Y (1982). "Motions of rigid bodies and criteria for overturning by earthquake excitations". *Earthquake Engineering and Structural Dynamics*, **10**(5): 635–650. https://doi.org/10.1002/eqe.4290100502
32. Spanos PD and Koh A (1984). "Rocking of Rigid Blocks Due to Harmonic Shaking". *Journal of Engineering Mechanics*, **110**(11): 1627–1642. https://doi.org/10.1061/(ASCE)0733-9399(1984)110:11(1627)
33. Priestley MJN, Evison RJ and Carr AJ (1978). "Seismic response of structures free to rock on their foundations". *Bulletin of the New Zealand Society for Earthquake Engineering*, **11**(33): 141–150. https://doi.org/10.5459/bnzsee.11.3.141-150
34. Bachmann JA, Strand M, Vassiliou MF, Broccardo M and Stojadinović B (2018). "Is rocking motion predictable?". *Earthquake Engineering and Structural Dynamics*, **47**(2): 535–552. https://doi.org/10.1002/eqe.2978
35. Mathey C, Feau C, Politopoulos I, Clair D, Baillet L and Fogli M (2016). "Behavior of rigid blocks with geometrical defects under seismic motion: an experimental and numerical study". *Earthquake Engineering and Structural Dynamics*, **45**(15): 2455–2474. https://doi.org/10.1002/eqe.2773
36. Makris N and Konstantinidis D (2003). "The rocking spectrum and the limitations of practical design methodologies". *Earthquake Engineering and Structural Dynamics*, **32**(2): 265–289. https://doi.org/10.1002/eqe.223
37. Bao Y and Konstantinidis D (2020). "Dynamics of a sliding-rocking block considering impact with an adjacent wall". *Earthquake Engineering and Structural Dynamics*, **49**(5): 498–523. https://doi.org/10.1002/eqe.3250

38. Vassiliou MF, Mackie KR and Stojadinović B (2014). "Dynamic response analysis of solitary flexible rocking bodies: Modeling and behavior under pulse-like ground excitation". *Earthquake Engineering and Structural Dynamics*, **43**(10): 1463–1481. https://doi.org/10.1002/eqe.2406
39. Linde SA, Konstantinidis D and Tait MJ (2020). "Rocking response of unanchored building contents considering horizontal and vertical excitation". *Journal of Structural Engineering*, **146**(9): 04020175. https://doi.org/10.1061/(ASCE)ST.1943-541X.0002735
40. Burningham C, Mosqueda G and Saavedra RR (2007). "Comparison of seismic fragility of free standing equipment using current testing protocols and recorded building floor motions". *Proceedings, Earthquake Engineering Symposium for Young Researchers*, Seattle (USA), Paper ID: 40207110. http://www.mceer.buffalo.edu/education/reu/2007/content/20Burningham.pdf
41. International Code Council Evaluation Service (ICC-ES) (2012). "*Acceptance Criteria for the Seismic Qualification of Nonstructural Components"*. ICC-ES, AC156, Brea (USA), 1-8. https://icc-es.org/acceptance-criteria/ac156/
42. Federal Emergency Management Agency (FEMA) (2007). "*Interim Protocols for Determining Seismic Performance Characteristics of Structural and Nonstructural Components through Laboratory Testing".* Applied Technology Council (ATC), FEMA 461, Washington (USA), 1-138. https://www.atcouncil.org/pdfs/FEMA461.pdf
43. D'Angela D, Magliulo G and Cosenza E (2021). "Towards a reliable seismic assessment of rocking components". *Engineering Structures*, **230**: 111673. https://doi.org/10.1016/j.engstruct.2020.111673
44. Porter K (2019). "*A Beginner's Guide to Fragility, Vulnerability, and Risk*". University of Colorado Boulder, Denver (USA), 1-139. https://www.sparisk.com/pubs/Porter-beginnersguide.pdf
45. Wittich CE and Hutchinson TC (2014). "Development of a rocking-period centered protocol for shake table testing of unattached stiff components". *Tenth US National Conference on Earthquake Engineering. Frontiers of Earthquake Engineering*, 2014, Anchorage (USA). https://doi.org/10.4231/D3BN9X373
46. D'Angela D, Magliulo G and Cosenza E (2019). "ICC-ES AC156 protocol vs real records: seismic response of freestanding components". *4th International Workshop on the Seismic Performance of Non-Structural Elements (SPONSE)*, 2019, Pavia (Italy), Paper ID: 21. https://doi.org/10.7414/4sponse.ID.21
47. Applied Technology Council (ATC). *"Quantification of Building Seismic Performance Factors"*. ATC, ATC-63 FEMA P-695, California (USA). https://www.atcouncil.org/atc-63
48. Center for Engineering Strong Motion Data (CESMD). *Center for Engineering Strong Motion Data 2017*. www.strongmotioncenter.org (Accessed October 2017)
49. The MathWorks Inc. (2018). *Matlab 9.5*.
50. Giouvanidis AI and Dimitrakopoulos EG (2018). "Rocking amplification and strong-motion duration". *Earthquake Engineering and Structural Dynamics*, **47**(10): 2094–2116. https://doi.org/10.1002/eqe.3058
51. Čeh N, Jelenić G and Bićanić N (2018). "Analysis of restitution in rocking of single rigid blocks". *Acta Mechanica*, **229**(11): 4623–4642. https://doi.org/10.1007/s00707-018-2246-8
52. Tsantaki S, Adam C and Ibarra LF (2017). "Intensity measures that reduce collapse capacity dispersion of P-delta vulnerable simple systems". *Bulletin of Earthquake Engineering*, **15**(3): 1085–1109. https://doi.org/10.1007/s10518-016-9994-4
53. Magliulo G, Maddaloni G and Petrone C (2013). "A procedure to select time-histories for shaking table tests on nonstructural components". *Proceedings of the 4th ECCOMAS Thematic Conference on Computational Methods in Structural Dynamics and Earthquake Engineering*, 2013, Paper ID: 1720. https://doi.org/10.13140/2.1.4693.8881
54. Petrone C, Magliulo G and Manfredi G (2017). "Shake table tests on standard and innovative temporary partition walls". *Earthquake Engineering and Structural Dynamics*, **46**(10): 1599–1624. https://doi.org/10.1002/eqe.2872
55. Petrone C, Magliulo G and Manfredi G (2016). "Floor response spectra in RC frame structures designed according to Eurocode 8". *Bulletin of Earthquake Engineering*, **14**(3): 747–767. https://doi.org/10.1007/s10518-015-9846-7
56. Wilcoski J, Gambill J and Smith S (1997). "*CERL Equipment Fragility and Protection Procedure (CEFAPP)"*. USACERL, Report 97/58. Champaign (USA), 1-140. https://apps.dtic.mil/
57. Wittich CE and Hutchinson TC (2015). "Shake table tests of stiff, unattached, asymmetric structures: Shake table tests of stiff, unattached, asymmetric structures". *Earthquake Engineering and Structural Dynamics*, **44**(14): 2425–2443. https://doi.org/10.1002/eqe.2589
58. Peña F, Prieto F, Lourenço PB, Campos Costa A and Lemos JV (2007). "On the dynamics of rocking motion of single rigid-block structures". *Earthquake Engineering and Structural Dynamics*, **36**(15): 2383–2399. https://doi.org/10.1002/eqe.739
59. Haymes K, Sullivan T and Chandramohan R (2020). "A practice-oriented method for estimating elastic floor response spectra". *Bulletin of the New Zealand Society for Earthquake Engineering*, **53**(3): 116–136. https://doi.org/10.5459/bnzsee.53.3.116-136
60. Málaga-Chuquitaype C, Psaltakis ME, Kampas G and Wu J (2019). "Dimensionless fragility analysis of seismic acceleration demands through low-order building models". *Bulletin of Earthquake Engineering*, **17**(7): 3815–3845. https://doi.org/10.1007/s10518-019-00615-2